



Enhancing of piezoelectric coefficient and optical Properties of flexible ZnO/Poly (Vinylidene Fluoride-Trifluoroethylene) Nanocomposites for Optoelectronic Applications

A. Hassan, A. Sarhan, M. I. Abdelhamid, T. Fahmy and A. Habib*



Polymer research group, Phys. Dept., Faculty of Sci. Mansoura University, 35516 Mansoura, Egypt

Abstract

The casting method is employed to produce the nanocomposite samples of ZnO/poly (vinylidene fluoride-trifluoroethylene) PVDF-TrFE with various contents of ZnONPs. Various techniques such as FTIR, XRD, DSC, UV-Vis and TGA are used to advance appreciation of the microstructure of PVDF-TrFE after embedding of ZnO nanoparticles. XRD showed that the electroactive b-phase fraction is enhanced and other parameters describe the crystalline structure like size of crystals, internal strain of lattice and density of dislocation are estimated. Analysis of FTIR spectra showed an interaction between PVDF-TrFE and ZnONPs and this explained the enhancement and growth of the electroactive b-phase fraction. DSC measurements showed that the temperature of ferroelectric to paraelectric phase transition is reduced from 404 K for PVDF-TrFE to 377 K for 1.25 wt% ZnO/PVDF-TrFE nanocomposite sample. TGA analysis of PVDF-TrFE revealed that with rising the content of ZnO NPs, the thermal stability enhanced. The impact of ZnO NPs on the behavior of the optical properties like absorbance, refractive index (n), extinction coefficient (k), indirect and direct optical band gap energy (E_{ig} and E_{dg}), oscillator and dispersion energies (E_o and E_d), oscillator strength (f) and parameters of nonlinear and linear optical (NLO) of ZnO/PVDF-TrFE nanocomposites are investigated in more details. The improvement of nonlinear optical parameters recommends them to be applied in various applications of nonlinear optical devices and optoelectronics.

KeyWords: PVDF-TrFE, β -polar phase, Band gap, harvesting energy, Piezoelectric coefficient.

1. Introduction

PVDF and their copolymers are electroactive fluoropolymers and this family is known for its unique piezoelectric and ferroelectric properties. Ability of these materials to convert mechanical stress into electrical charge and vice versa makes them suitable for many applications in soft and flexible electronics [1-3]. PVDF is a semi-crystalline polymer and crystallizes in various phases, i.e. α , β , γ , δ and ϵ -phase. α -phase has a chain conformation

of TGTG/ and γ phase has a TTTGTTG/ conformational pattern with lower piezoelectricity than β phase. β -phase has a higher piezoelectric activity since the polymer chain containing monomer of (CH₂-CF₂) units align as all-trans (TTTT) conformation. Also, owing to large difference in electronegativity between hydrogen and fluorine atoms and carbon atoms, a strong dipole moment will arise, resulting in macroscopic polarization within the material [4, 5]. After the synthesis process PVDF is obtained in mainly non-polar α -phase. However, it can be converted into β phase under high pressure through many complex treatments like

*Corresponding author e-mail: ahmedhabib@mans.edu.eg; (Ahmed Habib).

Received date 29 April 2023; revised date 06 June 2023; accepted date 11 June 2023

DOI: 10.21608/EJCHEM.2023.207514.7913

©2023 National Information and Documentation Center (NIDOC)

crystallization, mechanical deformation or doping with other materials [6]. In order to avoid such procedures, PVDF-TrFE copolymer is used which crystallizes to a crystalline structure often similar to β -phase facilitating the preparation of the electroactive polymer thin film. The addition of the co-monomer of trifluoroethylene (TrFE) into the VDF directly show enhancement of PVDF-TrFE copolymer crystallinity in β -phase without the need for mechanical pretreatment. The ratio of TrFE in the copolymer will determine the crystal structure while VDF content controls the electrical structure stability. At molar concentrations above 11% of TrFE, defects due to the existence of bulky fluorine will prevent trans-gauche formation of paraelectric α -phase (hexagonal conformation) phase under Curie temperature (T_c) [7, 8].

Currently, nanocomposite materials are attracting a lot of attention because of its noteworthy optical and piezoelectric properties [9-11]. Nanocomposites with novel and unique properties can be obtained by successfully combining the properties of the main components of these materials in one material. These materials, whether pure organic polymers or inorganic nanoparticles (INPs), differ with certain optical and electronic properties, are therefore widely used in optical applications such as light-emitting diodes (LEDs), optical guides, lenses, optical switches, and nonlinear optical instruments [12]. Incorporation of INPs into an organic polymer exhibits unique properties that enhance several physical properties of nanocomposites, which are different from those of ordinary materials [13, 14]. Significant and obvious changes in these properties can be observed even for a very small nanoparticles (NPs) fraction.

Some reports in a literature revealed that by adding of ZnO NPs to an organic polymer improved the electronic and optical behavior of the polymer due to the interfacial interaction between organic polymer and INPs [15-17]. As well known, ZnO is a semiconductor nonlinear optical nanomaterial with energy bandgap of 3.3 eV having a Wurtzite hexagonal structure with exciting applications in the field of optoelectronics technology such as solar cells, light-emitting diodes (LEDs), sensors, transparent conductors and piezoelectricity [12, 18]. Hence nanocomposite of ZnO/PVDF-TrFE can be used as UV shielding due to its superior absorption capacity.

Our present study aimed to investigate the influence of ZnONPs on the structural, optical and piezoelectricity properties of ZnO/PVDF-TrFE nanocomposite samples with different ZnO NPs content. This study is mainly focused on the analysis

of XRD pattern, FTIR spectra, absorption spectrum, optical bandgap, nonlinear optical parameters, thermal degradation and piezoelectric activity of PVDF-TrFE doped with different ZnO concentrations.

2. Experimental Work

2.1 Materials

PVDF-TrFE copolymer powder with 65 mol% of VDF and 35 mol% of TrFE is supplied from Solvay (Belgium). ZnO nanoparticles is supplied and synthesized in polymer laboratory, physics department, Mansoura University with crystal size of 32 nm [19]. Dimethyl formamide (DMF) is supplied from El Nasr pharmaceutical chemical co. (Egypt).

2.2 Preparation method

PVDF-TrFE and ZnO NPs are dissolved separately at 323 K under continuous stirring in DMF until completely dissolved. Then both solutions are mixed and stirred for 2 hours, then sonicated for 30 min. The resulting mixture is then poured at 373 K on a glass petri dish for three hours in an oven until the solvent volatilized, then the film was ready for measurements. The obtained samples have a circular shape with a diameter of 1 cm and a thickness in the range of 30-50 μ m,

2.3 Characterization tools

Measurements of XRD pattern are performed by a Bruker D8 advance powder XRD with a Cu K_{α} radiation source ($\lambda = 1.5418 \text{ \AA}$) at a current of 50 mA and voltage of 40 kV. The rate of scan is $3^{\circ}/\text{min}$ in the range of 2θ from 5° to 70° . ATR-FTIR spectra carried out at room temperature in ambient air in the wavenumber range from 4000 to 400 cm^{-1} using Thermo Scientific iD5 ATR spectrometer with a spectral resolution of 1 cm^{-1} . Measurements of differential scanning calorimetry (DSC) are performed by NETZSCH STA 409C/CD instrument in a range of temperature from 300K to 500K with rate of heating of $\sim 10 \text{ K/min}$. Measurements of thermogravimetric analysis (TGA) are obtained using TGA-50 SHIMADZU thermogravimetric analyzer with temperature range from 303 K to 1073 K. UV-

Vis spectra are measured with wavelength range extends from 200 to 1100 nm using an ATI Unicam UV-Vis spectrophotometer (Mattson Co.).

Piezoelectric activity measurements are performed at various stresses from 2.45×10^5 to 6.24×10^5 Pa by applying different loads at different measuring temperature T_m from 313K to 353K on the samples which are polarized by a fixed electric polarizing field $E_p = 1 \times 10^7$ V/m at polarized temperature $T_p = 353$ K for polarized time $t_p = 20$ min. Using Keithley 610c electrometer, the piezoelectric current is measured. The sample temperature is controlled and measured by a temperature controller system (Digi-Sence, Cole-Parmer Co., USA)

3. Results and Discussion

3.1 XRD

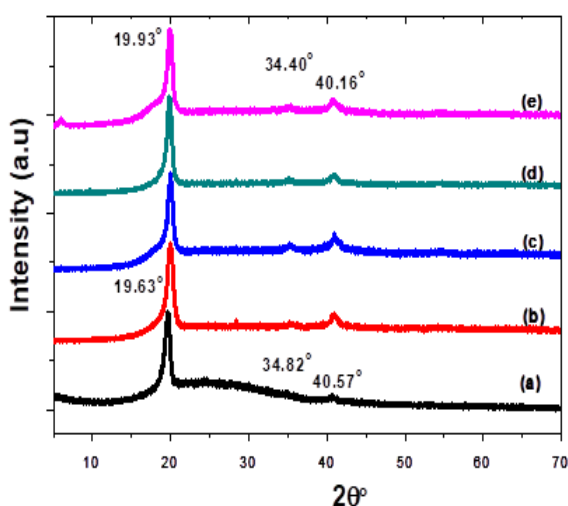


Fig. 1: XRD pattern of a) pure PVDF-TrFE and ZnO/PVDF-TrFE with several contents of ZnONPs b) 0.5 wt%, c) 0.75 wt%, d) 1 wt% and e) 1.25 wt%.

XRD measurements are performed to identify b-phase crystal structure in the nanocomposite samples. Fig. 1 illustrates XRD pattern of pure PVDF-TrFE and ZnO/PVDF-TrFE nanocomposite samples. The diffraction peaks at $2\theta = 19.68^\circ$ and 34.82° of β -phase in PVDF-TrFE with (110)/(200) and (020) planes are observed, as shown in Fig. 1a, confirming the semicrystalline nature of PVDF-TrFE [20].

The diffraction peak at 34.82° corresponds to the orthorhombic b-phase crystal, confirming the existence of the ferroelectric b-phase [21]. Upon doping with ZnO NPs a slight change in the intensity and position of β -phase diffraction peaks in the highly doped sample of ZnO/PVDF-TrFE nanocomposites is observed [22], as shown in Fig. 1e. These results indicate that the polar b-phase of PVDF-TrFE enhanced successively after doping with ZnO NPs. This means that these nanocomposites may show a better piezoelectric response [23]. The crystal size (D), internal lattice strain (ϵ) and intercrystallite distance (R) values of the investigated samples are computed using Debye-Scherrer equation as follows [24, 25]:

$$D = \frac{0.9 \lambda}{\beta \cos \theta} \quad (1a)$$

$$\epsilon = \frac{\beta_{hkl}}{4 \tan \theta} \quad (1b)$$

$$R = \frac{5 \lambda}{8 \sin \theta} \quad (1c)$$

where β , λ , θ are the wavelength, FWHM and diffraction angle, respectively. Various other structural parameters such as the number of crystallites per unit area (N_c) and the density of dislocation (δ) are estimated using the following expression [26,27]:

$$N_c = \frac{d}{D^3} \quad (2a)$$

$$\delta = \frac{1}{D^2} \quad (2b)$$

$$SF = \beta \left[\frac{2\pi}{45 (\tan \theta)^{0.5}} \right] \quad (2c)$$

where d is the sample thickness. The parameters of the structure calculated and listed in Table 1.

Table 1: Structural parameters of ZnO/PVDF-TrFE nanocomposites

Structural parameters	PVDF-TrFE	0.5 wt% ZnO/PVDF-TrFE	0.75 wt% ZnO/PVDF-TrFE	1 wt% ZnO/PVDF-TrFE	1.25 wt% ZnO/PVDF-TrFE
D (nm)	12.97	11.68	12.71	12.55	13.10
ϵ	1.64×10^{-3}	1.78×10^{-3}	1.63×10^{-3}	1.67×10^{-3}	1.59×10^{-3}
R (Å)	5.66	5.56	5.54	5.58	5.56
N_c (nm ⁻²)	22.86	31.32	24.29	25.29	22.22
δ (nm ⁻²)	5.93×10^{-4}	7.32×10^{-4}	6.18×10^{-4}	6.34×10^{-4}	5.82×10^{-4}
SF	0.030	0.033	0.030	0.031	0.029

3.2 FTIR Spectroscopy

FTIR spectra of PVDF-TrFE and ZnO/PVDF-TrFE nanocomposites with various concentrations of ZnONPs in the region 1600-400 cm^{-1} are given in Fig. 2. FTIR spectrum of pure PVDF-TrFE showed many absorption bands such as 1426, 1402, 1184, 1122, 1079, 884, 846, 506 and 478 cm^{-1} . The absorption bands at 1426, 1122, 884 and 846 cm^{-1} are related to β -phase. These vibration bands confirmed the existence of ferroelectric β -phase in the PVDF-TrFE copolymer [28].

where A_α is the intensity of absorption peak of α -phase at 772 cm^{-1} and A_β is the intensity of β phase at 846 cm^{-1} . Also, K_α and K_β are the absorption coefficients of these respective bands and equal 6.1×10^4 and $7.7 \times 10^4 \text{ cm}^2 \text{ mol}^{-1}$, respectively [30].

It is found that, the electroactive β -phase fraction has been enhanced and increased from 87.22% of pure PVDF-TrFE to 91.3 % for 1 wt% ZnO/PVDF-TrFE nanocomposite sample.

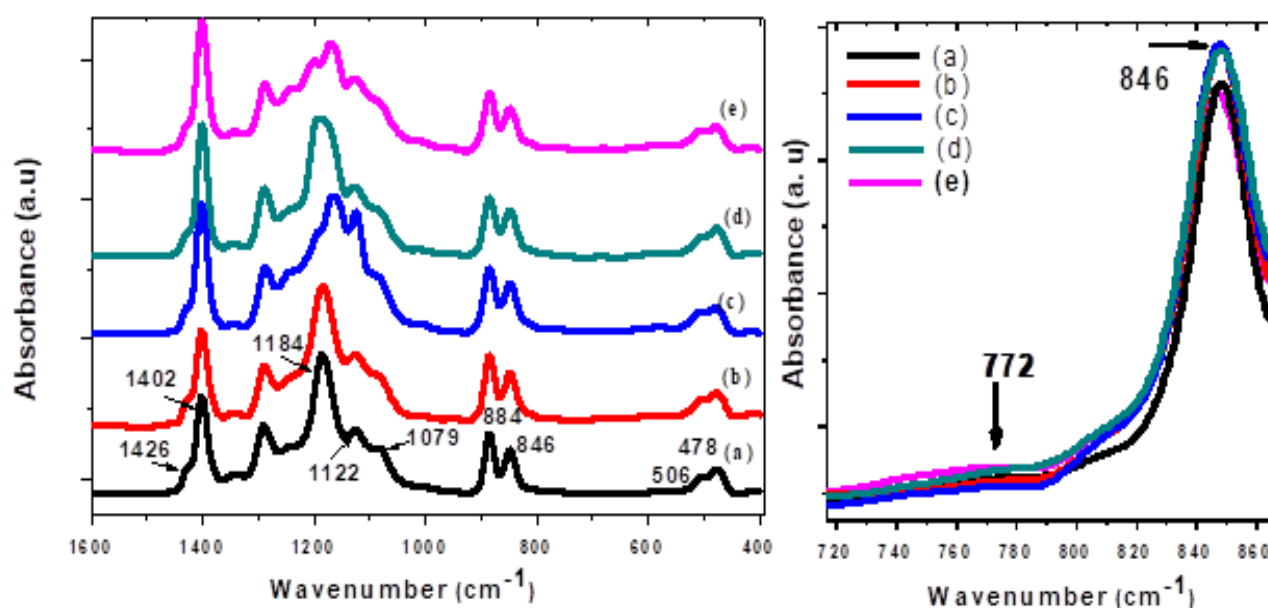


Fig. 2: FTIR spectra of a) pure PVDF-TrFE and ZnO/PVDF-TrFE with different concentrations of ZnONPs b) 0.5 wt%, c) 0.75 wt%, d) 1 wt% and e) 1.25 wt%.

Band at 1402 cm^{-1} is related to the combination between α , β and γ phases [29]. The band of absorption at 1079 cm^{-1} is ascribed to combination of β and γ phases [30]. The band at 478 cm^{-1} is attributed to α phase [20]. Upon doping with ZnO NPs the intensity of vibration bands characterizing the β -phase are increased in comparison to the bands of α -phase with increasing ZnO NPs content. The electroactive β -phase fraction $F(\beta)$ in the nanocomposites is computed with follows [31]:

$$F(\beta) = \frac{A_\beta}{(K_\beta/K_\alpha)A_\alpha + A_\beta} \quad (3)$$

3.3 Differential scanning calorimetry (DSC) analysis

DSC measurements of ZnO/PVDF-TrFE nanocomposites are carried out in the temperature range from 300 to 490 K with rate of heating of 10 K/min as given in Fig. 3. The ferroelectric to paraelectric transition (T_c) peak of the pure PVDF-TrFE is observed at 404 K and reduced to be 377 K for 1.25 wt% ZnO/PVDF-TrFE nanocomposite sample. The endothermic peak at 423 K is related to the melting temperature (T_m) of the crystalline phase of PVDF-TrFE [7]. As illustrated in Fig. 3, a noticeable decreasing in the melting point of PVDF-TrFE than that of ZnO/PVDF-TrFE nanocomposite

samples is observed. The broader endothermic peak of pure PVDF-TrFE which is observed at around 423 K shifted towards lower (T_m) values for ZnO/PVDF-TrFE nanocomposites. The lowest T_m value is obtained at around 417 K for the highly doped sample. The increase of ZnO NPs content will decrease the intermolecular interaction between chains of PVDF-TrFE and thus the crystal structure of the PVDF-TrFE will disturb [33]. A significant reduction in the transition point of ferroelectric to paraelectric is observed with increasing the content of ZnO nanoparticles. The values of T_c and T_m of pure PVDF-TrFE and ZnO/PVDF-TrFE nanocomposites are given in Table 2.

Table 2: Values of T_c and T_m of ZnO/PVDF-TrFE nanocomposites.

Sample	T_c (K)	T_m (K)
PVDF-TrFE	404	423
0.5 wt% ZnO/PVDF-TrFE	380	418
0.75 wt% ZnO/PVDF-TrFE	380	418
1.0 wt% ZnO/PVDF-TrFE	378	418
1.25 wt% ZnO/PVDF-TrFE	377	417

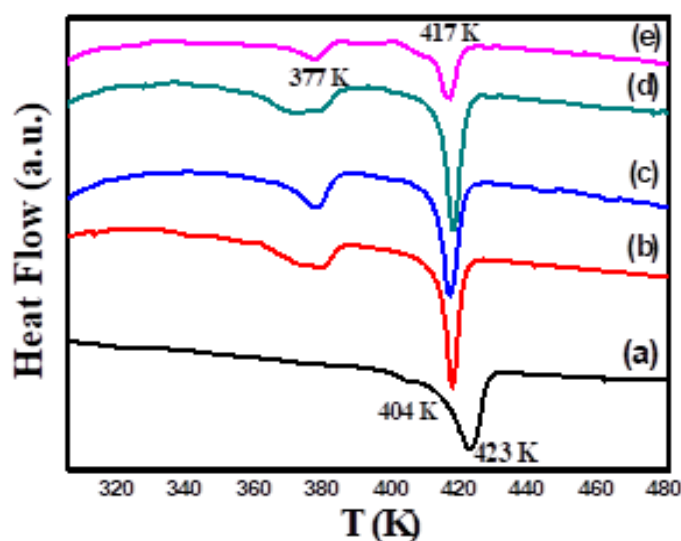


Fig. 3: DSC of a) PVDF-TrFE and ZnO/PVDF-TrFE with different concentration of ZnO NPs b) 0.5 wt%, c) 0.75 wt%, d) 1 wt% and e) 1.25 wt%.

Fig. 4 illustrates variation of weight losses and the first derivative (DTG) curves of ZnO/PVDF-TrFE nanocomposite samples. It is observed that pure PVDF-TrFE is very stable till temperature as high as 716 K. After that temperature, the degradation occurs in one stage with a weight loss of 98.42% at a maximum temperature of 762.5 K, as shown in Fig. 4a.

The process of thermal decomposition of PVDF-TrFE is described by scissions of C-F and C-H of the polymer main-chain, the scission of C-H is occurred in a first step as a result of C-F bond strength (460 kJ/mol) unlike C-H bond of (410 kJ/mol) [34]. The combination between fluorine and hydrogen atoms through the thermal decomposition process will promote the hydrogen fluoride (HF) formation. As a result of the loss of HF in the first stage, polyenic sequences are formed along the main polymer chain. Since these compounds are unstable, more scission reactions will occur leading to the aromatic volatile molecules are formed [35]. Also in the same vein some authors suggested the occurrence of backbone scission and small amount of $C_4H_3F_3$ is formed [36]. Fig. 4(b-e) displays TGA/DTG curves of ZnO/PVDF-TrFE nanocomposite samples. It is observed that the thermal degradation of these nanocomposites is occurred through two stages with higher value of maximum temperature compared to PVDF-TrFE. The values of weight loss and maximum temperature of each degradation stage is given in Table 3. Our data in Table 3 revealed that the thermal stability PVDF-TrFE has been enhanced due to the presence of ZnO NPs.

Table 3: Peak temperature (T_m) and mass loss (%) for PVDF-TrFE and ZnO/PVDF-TrFE nanocomposite samples.

Sample	Stage I		Stage II		Residual mass (%)
	T_m (K)	Mass loss (%)	T_m (K)	Mass loss (%)	
PVDF-TrFE	762.5	98.16	--	--	1.84
0.5 wt% ZnO/PVDF-TrFE	769.8	82.65	834.6	14.28	3.065
0.75 wt% ZnO/PVDF-TrFE	758.1	63.10	813.1	12.75	24.15
1.0 wt% ZnO/PVDF-TrFE	767.9	76.11	830.0	17.39	6.5
1.25 wt% ZnO/PVDF-TrFE	764.0	77.65	828.0	17.735	4.61

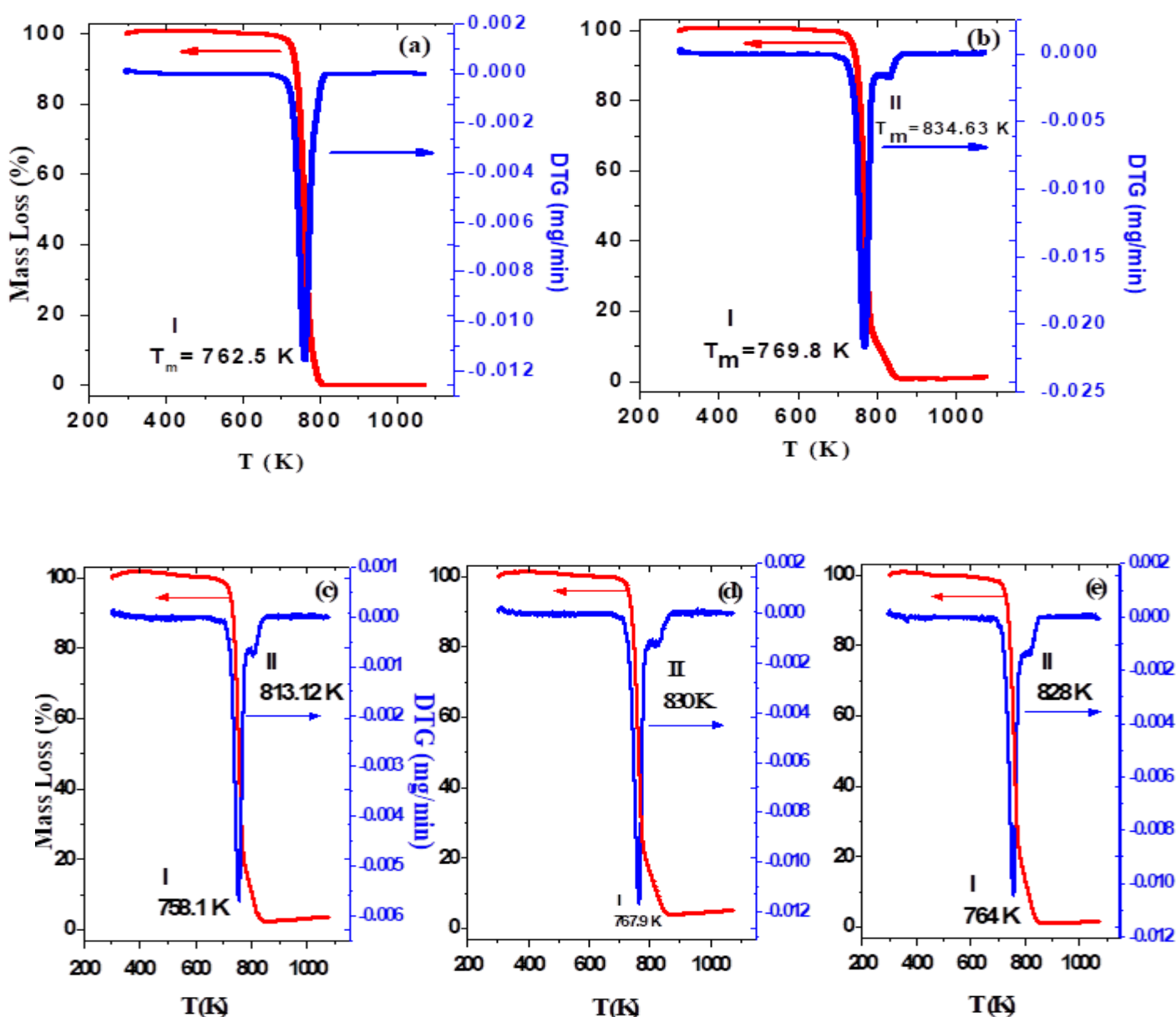


Fig. 4: TGA curve of a) PVDF-TrFE and ZnO/PVDF-TrFE with different concentration of ZnO NPs b) 0.5 wt%, c) 0.75 wt% d) 1 wt% and e) 1.25 wt%.

Thermogravimetric analysis (TGA) is widely used to investigate the kinetics of thermal degradation of polymer. In this context, the mass loss is recorded continuously as a function of increasing the temperature of the material. To give insight into the mechanism of the thermal degradation, various models are used. TGA provides the sample weight loss over time, which is converted to the fractional conversion (g) as follows [37]:

$$g = \frac{m_i - m_t}{m_i - m_f} \quad (4)$$

Where m_i is the primary sample mass, m_t is the mass at certain time (isothermal analysis) during the reaction and m_f is the final mass at the end of reaction, respectively. For polymer thermal degradation, a general solid-state reaction rate form

is expressed by fractional conversion related to time, rate constant and reaction model $f(\alpha)$. Kinetics of polymer degradation is expressed as follows [38]:

$$\frac{dg}{dt} = \beta \frac{dg}{dT} = k(T) f(g) \tag{5}$$

where β is the heating rate, $f(\alpha)$ is the conversion function and $k(T)$ is the rate constant. The rate constant, $k(T)$ in case of thermally stimulated process is expressed using Arrhenius equation as follow:

$$\frac{dg}{dt} = f \exp\left(-\frac{E_a}{RT}\right) f(g) \tag{6}$$

where E_a , R and f are the activation energy, gas constant and frequency factor, respectively. The frequency factor (f) can be described as follow [39]:

$$f = \frac{\delta e k_B T}{h} \exp\left(\frac{\Delta S}{R}\right) \tag{7}$$

where δ is the transmission coefficient and equals the unity for the monomolecular reaction, e is the Neper number ($e = 2.7183$), h is the Planck's constant and ΔS is the entropy activation, respectively. Therefore, the rate constant is described as follow:

$$k(T) = \frac{\delta e k_B T}{h} \exp\left(\frac{\Delta S}{R}\right) \exp\left(-\frac{E_a}{RT}\right) \tag{8}$$

The values of entropy activation (ΔS) can be calculated from eqn. (8) as follow:

$$\Delta S = 2.303 R \log\left(\frac{f h}{\delta e k_B T}\right) \tag{9}$$

and

$$E_a = \Delta H + RT \tag{10}$$

where, ΔH is the enthalpy activation and Gibbs free energy (ΔG) can be computed as follows

$$\Delta G = \Delta H - T \Delta S \tag{11}$$

The thermodynamic parameters (f , E_a , ΔS , ΔH , ΔG) of ZnO/PVDF-TrFE nanocomposite samples are calculated by using the Coats-Redfern approach, using the reaction order $n=1$, according to the following equation [40]:

$$\log\left[-\frac{\log(1-g)}{T^2}\right] = \log\left[\frac{fR}{\beta E_a}\left(1 - \frac{2RT}{E_a}\right)\right] - \frac{E_a}{2.303RT} \tag{12}$$

In case of $2RT/E_a \ll 1$, the eq. (12) will be in the following form [38]

$$\log\left[-\frac{\log(1-g)}{T^2}\right] = \log\left[\frac{fR}{\beta E_a}\right] - \frac{E_a}{2.303RT} \tag{13}$$

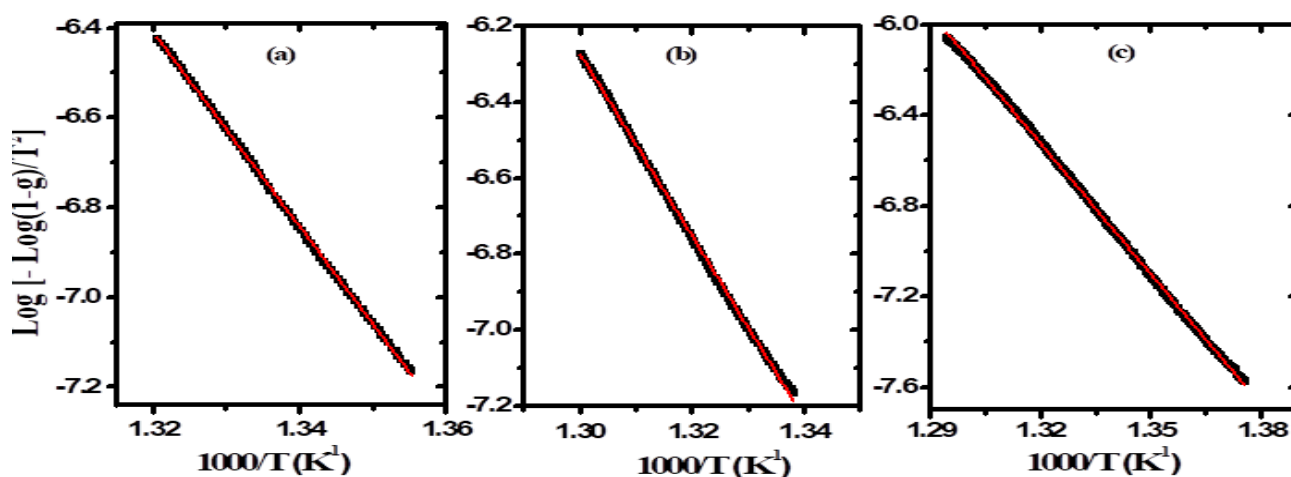


Fig. 5: Log $[-\log(1-g)/T^2]$ versus $1/T$ for a) pure PVDF-TrFE, b) 0.5 wt% ZnO/PVDF-TrFE and c) 1 wt% ZnO/PVDF-TrFE NCs.

Fig. 5(a-c) displays $\log[-\log(1-g)/T^2]$ versus $1/T$ for the investigated samples in the first stage of thermal decomposition. The plots result in straight lines with slope of $-E_a/2.303R$ from which values of E_a are estimated and the intercept of $\log(fR/\beta E_a)$ from which the frequency factor values are evaluated. The kinetic parameters of ZnO/PVDF-TrFE nanocomposites in the first and second stages are determined and given in Table 4. The higher values of E_a may be attributed to the reaction of the macromolecules with radicals and/or small molecular that present in the polymer [41].

Table 4: Thermodynamic parameters of ZnO/PVDF-TrFE with various concentration of ZnO NPs (0.5, 0.75, 1 and 1.25 wt %).

Stage I						
Samples	T_m (K)	E (kJ)	f (Hz)	ΔS (kJ/mol K)	ΔH (kJ/mol)	ΔG (kJ/mol)
PVDF-TrFE	488.0	382.06	1.22×10^{24}	0.21	378.01	277.75
0.5 wt% ZnO/PVDF-TrFE	769.8	405.04	2.52×10^{25}	0.23	398.65	221.14
0.75 wt% ZnO/PVDF-TrFE	758.0	396.82	2.39×10^{25}	0.23	390.52	216.08
1 wt% ZnO/PVDF-TrFE	767.9	367.39	9.39×10^{22}	0.18	361.01	219.66
1.25 wt% ZnO/PVDF-TrFE	762.5	343.68	2.51×10^{21}	0.15	337.35	219.95
Stage II						
0.5 wt% ZnO/PVDF-TrFE	834.63	53.982	11.32032005	-0.24	47.04	243.68
0.75 wt% ZnO/PVDF-TrFE	813.12	216.75	7.03374E+12	-0.01	210.00	217.96
1 wt% ZnO/PVDF-TrFE	830.0	54.041	10.37965431	-0.24	47.14	243.29
1.25 wt% ZnO/PVDF-TrFE	828.0	59.030	11.33780227	-0.24	52.15	247.21

The correlation between isokinetic rate constant (k_{iso}), isokinetic temperature (T_{iso}) and activation energy (E_a) is expressed as follows [40]

$$\ln f = \ln k_{iso} + \frac{E_a}{RT_{iso}} \quad (14)$$

Fig. 6a illustrates the variation of $\ln f$ versus E_a . The k_{iso} and T_{iso} values are calculated from the intercept of $(\ln k_{iso})$ and slope of $(1/RT_{iso})$, as shown in Fig. 6a. It is found that, the isokinetic rate constant (k_{iso}) in the order of 1.69×10^{-10} Hz and the isokinetic temperature (T_{iso}) in the order of 703.38 K. Also, a linear behavior between entropy and enthalpy is observed, as shown in Fig. 6b. Such behavior is called enthalpy-entropy compensation (EEC) effect. EEC effect has been reported previously using TGA/DTG analysis or thermally stimulated depolarization current technique for many polymers [43-45].

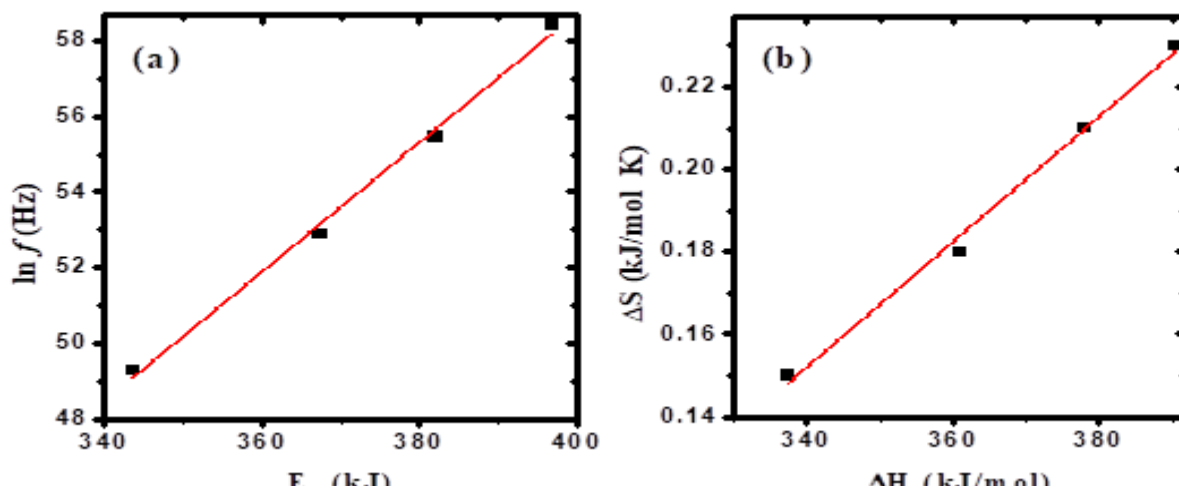


Fig. 6: a) $\ln f$ versus E_a and b) ΔS versus ΔH in the first stage.

3.5 UV-Vis Spectroscopy

3.5.1 Band gap energy

Fig. 7a illustrates the absorption spectra of PVDF-TrFE and ZnO/PVDF-TrFE nanocomposites in the range from 200 nm to 1100 nm. Spectrum of pure PVDF-TrFE displayed an absorption peak at 210 nm and shifted to 235 nm with increasing the content of ZnO nanoparticles. These bands are attributed to the π - π^* transition and the sharp absorption edge at 210 nm indicated the semicrystalline nature of PVDF-TrFE[46]. The spectrum of ZnO/PVDF-TrFE nanocomposites showed another absorption peak at 393 nm and related to ZnO[47].

Furthermore, it is observed that the absorbance of the nanocomposite samples changes and increases smoothly with increasing ZnO doping content because the combined filling of doping ions with PVDF-TrFE chains absorbs the incident radiation by free electrons at the shortest wavelengths. Therefore, from a chemical point of view, a significant change is occurred in the polymer structure. Fig. 7b displays the absorption coefficient α ($\alpha=2.303 A/d$, where A and d is the absorbance and sample thickness) variation of all samples versus the photon energy.

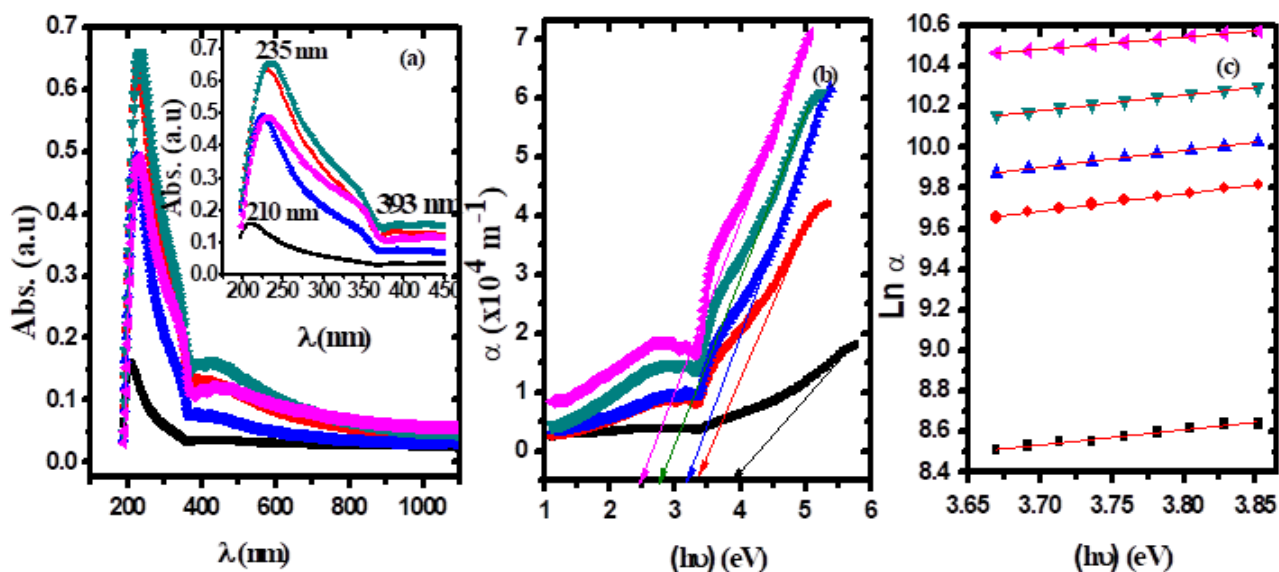


Fig. 7: a) The absorption versus λ b) α versus $h\nu$ and c) $\ln \alpha$ versus $h\nu$. (■) PVDF-TrFE, (●) 0.5 wt% ZnO/PVDF-TrFE, (▲) 0.75 wt% ZnO/PVDF-TrFE, (▼) 1 wt% ZnO/PVDF-TrFE and (◄) 1.25 wt% ZnO/PVDF-TrFE.

from 4.69 eV for pure PVDF-TrFE to 2.63 for 1.25 wt% ZnO/PVDF-TrFE nanocomposite sample. The absorption edge shift to the higher wavelengths reflects the change of the optical energy band gap, which may be due to the modification in the crystal phase of PVDF-TrFE matrix. The values of the absorption edge of all samples are given in Table 5. Near the absorption edge, the absorption coefficient (α) displays an exponential dependence on the energy of incident photons ($h\nu$) and this dependence is defined as Urbach rule. The Urbach energy (E_U) is computed as follows [48]:

$$\alpha = \alpha_0 \exp\left(\frac{h\nu}{E_U}\right) \quad (15)$$

where α_0 is a pre-exponential factor. The Urbach energy values will provide more details about the optical behavior of ZnO/PVDF-TrFE nanocomposite samples. Fig. 7c depicts the relation between photon energy ($h\nu$) and $\ln(\alpha)$. The values of Urbach energy are estimated by knowing the slope of the fitted straight lines and given in Table 5. It is shown that E_U values of composites increased with ZnO NPs content increased. This increase in Urbach energy values is indicative to the structure modification of PVDF-TrFE matrix,

which in turn will lead to an increasing in the disorder of the nanocomposites. These defects will create lower energy states leading to higher charge carrier concentration in the conduction band [12].

The nature of optical transitions in ZnO/PVDF-TrFE nanocomposites is investigated by Tauc equation as follows [47]:

$$\alpha h\nu = B(h\nu - E_g)^m \quad (16)$$

where B is a constant and m is an exponent describes the electronic transitions nature, i.e., for the direct allowed transition ($m=1/2$), indirect allowed transition ($m=2$), direct forbidden transition ($m=1/3$) and indirect forbidden transition ($m=3$), respectively. Fig. 8 illustrates the dependence of $(\alpha h\nu)^{0.5}$ and $(\alpha h\nu)^2$ on $h\nu$ for all samples. The values of direct (E_{dg}) and indirect (E_{ig}) optical band gap energy are calculated by extrapolate the linear portions of the curves of Figs. 8(a&b) to $(\alpha h\nu)^{0.5} = 0$ and $(\alpha h\nu)^2 = 0$ on the x-axis and given in Table 5. It is noted that both the indirect and direct energies are decreased with increasing content of ZnO, which contributes to the localized states near the band edge, which in turn reduces the Fermi level and hence affects the energy gap. The indirect and direct energies are reduced from 2.89 eV and 4.82 eV for pure PVDF-TrFE to 1.69 eV and 3.85 eV for 1.25 wt% ZnO/PVDF-TrFE, respectively. The reduction in the band gap is related to the structure modification after doping with ZnO nanoparticles [50].

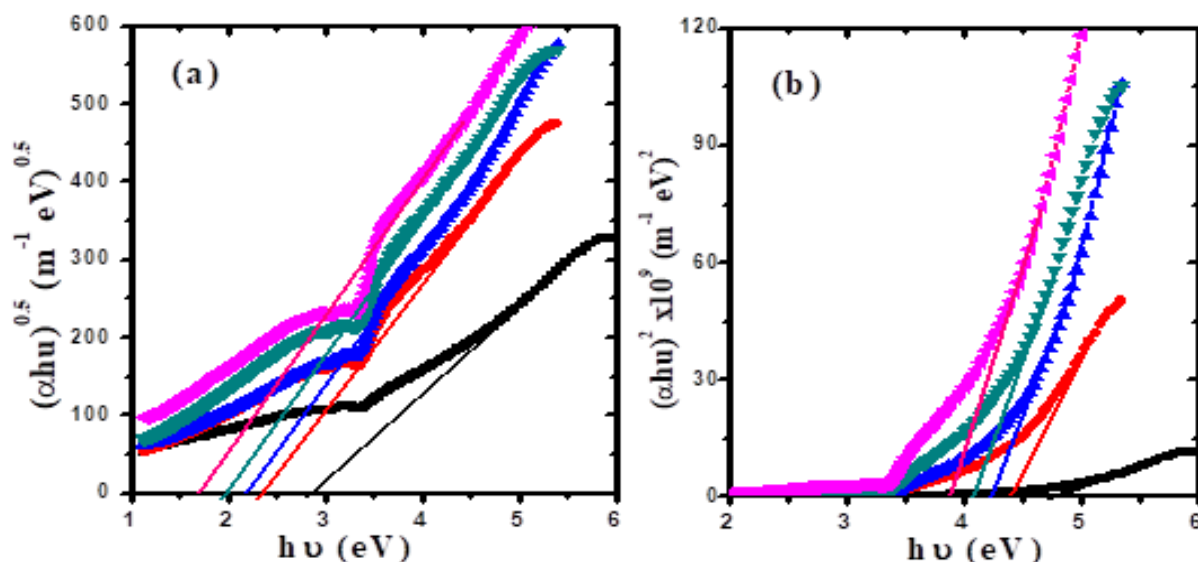


Fig. 8: a) $(\alpha h\nu)^{0.5}$ vs $h\nu$ and b) $(\alpha h\nu)^2$ vs $h\nu$. (■) PVDF-TrFE, (●) 0.5 wt% ZnO/PVDF-TrFE, (▲) 0.75 wt% ZnO/PVDF-TrFE, (▼) 1 wt% ZnO/PVDF-TrFE and (◆) 1.25 wt% ZnO/PVDF-TrFE.

The decrease in the values of optical energy is related to the defect's formation and thus the optical behavior of the material will be affected. The optical bandgap reduction can strongly nominate ZnO/PVDF-TrFE nanocomposites for use as absorbent layer in the solar cell to enhance the photovoltaic devices efficiency.

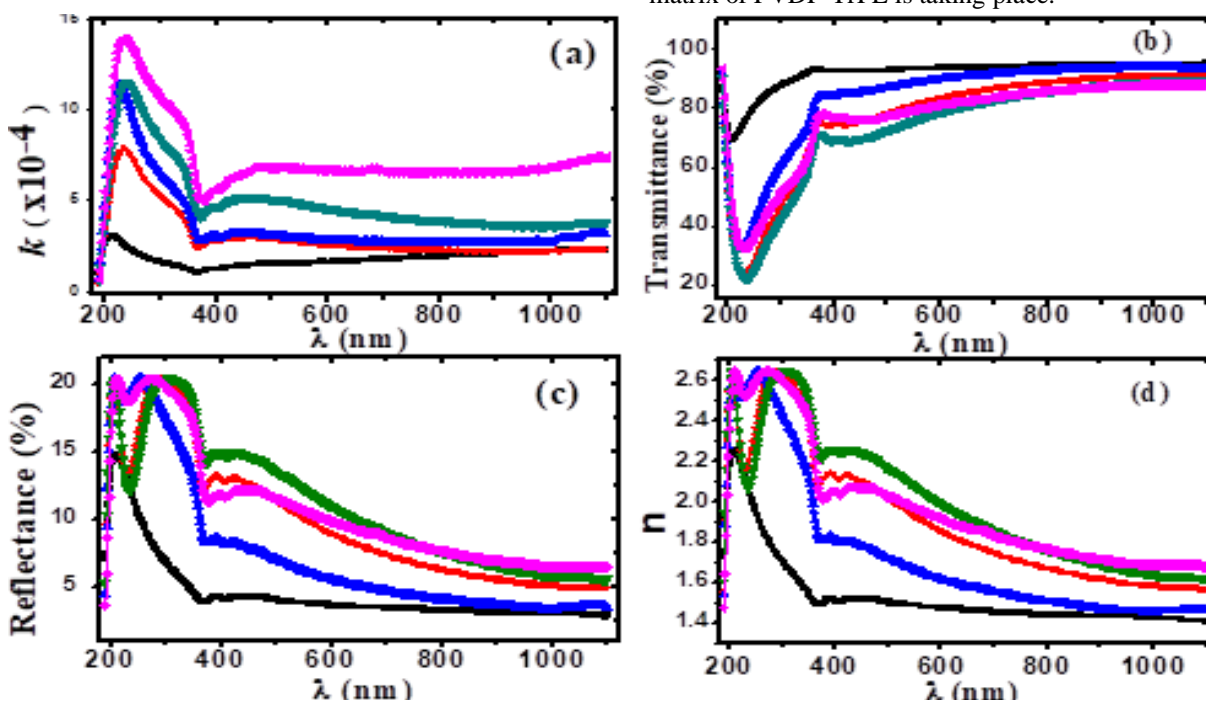


Fig.9: a) The absorption index against λ b) T (%) against λ c) R (%) against λ and d) n against λ . (■) PVDF-TrFE, (●) 0.5 wt% ZnO/PVDF-TrFE, (▲) 0.75 wt% ZnO/PVDF-TrFE, (▼) 1 wt% ZnO/PVDF-TrFE and (◄) 1.25 wt%

The absorption index measures of the fraction of light lost within a material owing to the processes of absorption and scattering and can be calculated as follows:

$$k = \frac{\alpha \lambda}{4\pi} \quad (17)$$

Fig. 9a displays the variation of k against wavelength for PVDF-TrFE and ZnO/PVDF-TrFE nanocomposites. It is clear that in the UV region the absorption index is decreased with increasing wavelength, while in the visible region it starts to increase again with increasing wavelength and it also increases with increasing ZnO NPs content. The incident photons have enough energy in the UV region for exciting the electrons to overcome the band gap, so the k values will reduce. This reduction in the values of k confirmed that the electromagnetic wave is allowed to pass in this region through ZnO/PVDF-TrFE nanocomposites without any

damping. On the other hand, the raise of the values of k with the increasing of ZnO NPs content in the visible region because energy of photon cannot produce an excitation of the electrons to transit from lower state to upper. Hence this energy will be lost due to collisions and scattering, i.e., more scattering of photons with increasing ZnO NPs content in the matrix of PVDF-TrFE is taking place.

Similar behavior has been reported previously for various polymeric composite materials [11, 44, 51].

Fig. 9b shows the variation of the transmittance (%) against the wavelength ZnO/PVDF-TrFE nanocomposites. It is found that in the visible region, the pure PVDF-TrFE is strongly transparent with transmittance of $\sim 95\%$. PVDF-TrFE nanocomposites showed similar behavior of PVDF-TrFE, however, with lower transmittance values of $\sim 82\%$. The reduction in the transmittance of nanocomposite samples may be attributed to the fact that ZnO nanoparticles act as scattering centers in the matrix of PVDF-TrFE. On the other side, the reflectance (R%) displays an opposite trend to transmittance behavior, as shown in Fig. 9c. Moreover, it increases with increasing the concentration of ZnO NPs in the visible region. The variations of transmittance and reflectance with increasing content of ZnO NPs in the nanocomposites may be explained based on the

proportional relationship between number of carriers and absorption of free carrier in the polymer matrix. the greater of absorption in the UV and visible regions with increasing of carriers number [44].

The refractive index (n) is an important parameter of the polymeric material that has a potential role in most applications of the optical devices. The refractive index depends mainly on the bond's strength, molecular weight, density of sample and is calculated using the following equation:

$$n = \left(\frac{1+R}{1-R} \right) + \sqrt{\frac{(1+R)^2}{(1-R)^2} - (1-k)^2}$$

$$R = 1 - \sqrt{T \exp(A)} \quad (18)$$

where R is the reflectance, A is the absorbance and T is the transmittance [52]. Fig. 9d illustrates the change of n with λ ZnO/PVDF-TrFE nanocomposites. It is found that n is decreased with increasing λ (dispersion behavior) for all investigated samples and tends to be constant at higher wavelength. Furthermore, the refractive index of PVDF-TrFE is enhanced with increasing the content of ZnO NPs and in the visible range reached to a highest value. The increase of n from 1.43 for PVDF-TrFE to 1.88 for 1.25 wt% ZnO/PVDF-TrFE at $\lambda = 700$ nm, can be interpreted with higher density of the nanocomposite samples with increasing the content of ZnO NPs.

3.5.2 Single Oscillator Model (SOM)

Dispersion of the refractive index is interpreted based on single oscillator model (SOM) which is introduced by Wemple and Domenico [53]. The correlation between refractive index and energy of the incident photon is expressed as follows:

$$(n^2 - 1)^{-1} = \frac{E_0}{E_d} - \frac{1}{E_d E_0} (h\nu)^2 \quad (18)$$

Where E_0 is the oscillator energy and expresses the average excitation energy of the electronic transition and E_d is the dispersion energy which is a determine of the interband optical transitions strength. The dispersion parameters (E_0 and E_d) of ZnO/PVDF-TrFE nanocomposites are estimated easily by plotting $(n^2-1)^{-1}$ versus $(h\nu)^2$, as shown in Fig. 10a. Values of E_0 and E_d are calculated from the intercept (E_0/E_d) and slope of $(E_0 E_d)^{-1}$ of the fitted lines of Fig. 10a, and given in Table 5. The values E_0 and E_d are found to be ranged from 4.80 to 2.78 eV and 4.63 to 7.80 eV. The change in E_0 values is ascribed to the electronic transitions between valance and conduction bands. Furthermore, other optical parameters can be computed by the values of E_0 and E_d as follows:

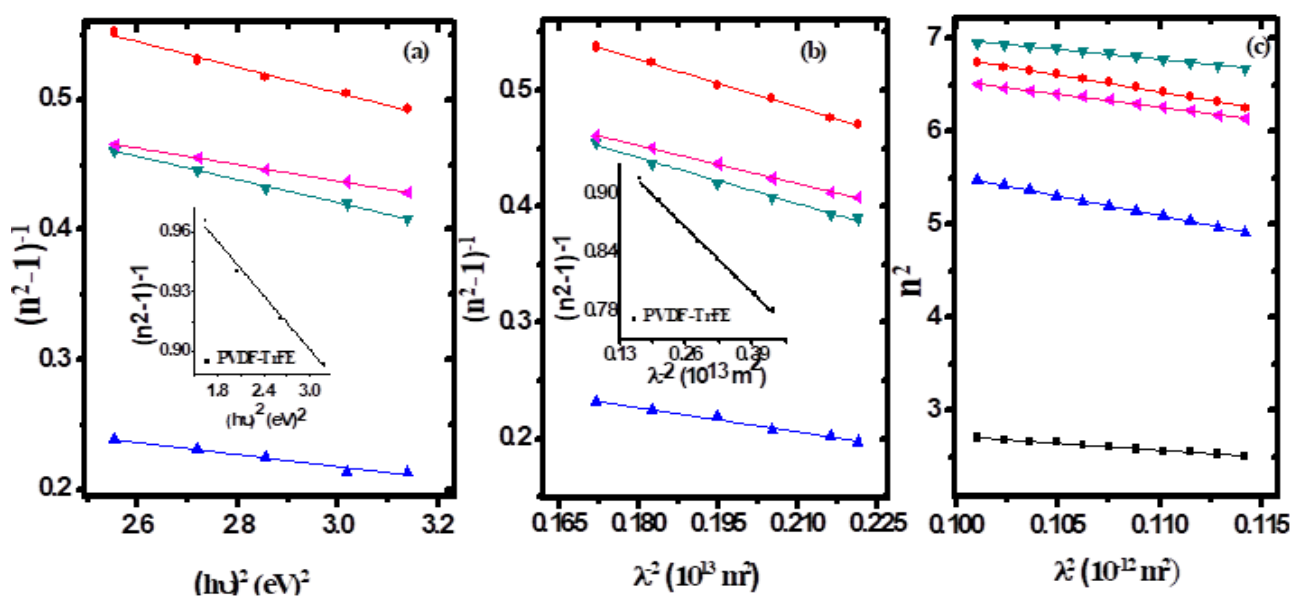


Fig. 10: a) $(n^2-1)^{-1}$ against $(h\nu)^2$ b) $(n^2-1)^{-1}$ against λ^2 and c) n^2 against λ^2 . (■) PVDF-TrFE, (●) 0.5 wt% ZnO/PVDF-TrFE, (▲) 0.75 wt% ZnO/PVDF-TrFE, (▼) 1 wt% ZnO/PVDF-TrFE and (◄) 1.25 wt% ZnO/PVDF-TrFE.

$$f = E_0 E_d$$

$$n_0 = \left(1 + \frac{E_d}{E_0} \right)^{1/2} \quad (19)$$

$$\varepsilon_s = n_0^2$$

where f represents the strength of the interaction between the material and electromagnetic radiation [53], n_0 is the static refractive index and ε_s is the static dielectric constant, respectively. All the parameters are estimated and listed in Table 5. It is noted that the (n_0) and (ε_s) values are enhanced and changed from 1.40 to 1.61 and from 1.97 to 2.59 with increasing ZnO NPs content.

Based on the Clausius-Mossotti concept, the molecular polarizability (η) and polarizability volume (η') of ZnO/PVDF-TrFE nanocomposites are computed and listed in Table 5 using the following equations [44, 54]

$$\eta = \frac{3M_w \varepsilon_0 (\varepsilon_s - 1)}{\rho N_A (\varepsilon_s + 2)} \quad \text{and} \quad \eta' = \frac{\mu}{4\pi \varepsilon_0} \quad (21)$$

where M_w is the molecular weight, ρ is the density and N_A is Avogadro's number, respectively. It is noted that μ and μ' values are enhanced and increased with increasing ZnO content. Since the electronic polarization is correlated to the molecular size, i.e., the increase in the molecular volume will lead to an increase of the polarizability volume [55].

Table 5: Optical and dispersion parameters values of ZnO/PVDF-TrFE nanocomposites

Optical Parameters	PVDF-TrFE	0.5 wt% ZnO/PVDF-TrFE	0.75 wt% ZnO/PVDF-TrFE	1.0 wt% ZnO/PVDF-TrFE	1.25 wt% ZnO/PVDF-TrFE
E_{ed} (eV)	3.84	3.42	3.14	2.80	2.42
E_U (eV)	1.34	1.16	1.22	1.29	1.67
E_{ig} (eV)	2.89	2.33	2.16	1.97	1.69
E_{dg} (eV)	4.82	4.35	4.24	4.05	3.85
M	44	61	63	66	74
Dispersion Parameters					
E_0 (eV)	4.80	2.85	2.79	2.78	3.15
E_d (eV)	4.63	3.57	7.80	4.04	5.03
f (eV) ²	22.22	10.20	21.73	11.23	15.87
n_0	1.40	1.50	1.95	1.57	1.61
ε_s	1.97	2.25	3.80	2.45	2.59
M_{-1}	0.982	1.118	1.673	1.206	1.262
M_{-3} , (eV) ⁻²	0.042	0.136	0.215	0.156	0.126
μ (x10 ⁻³⁷ Cm ² V ⁻¹)	3.97x10 ⁻³⁸	4.79x10 ⁻³⁸	7.88x10 ⁻³⁸	5.33x10 ⁻³⁸	5.66x10 ⁻³⁸
μ' (x10 ⁻²⁷ m ³)	3.57x10 ⁻²⁸	4.31x10 ⁻²⁸	7.08x10 ⁻²⁸	4.79x10 ⁻²⁸	5.09x10 ⁻²⁸
ε_L	4.22	10.43	9.73	9.13	9.34
N/m^* (m ⁻³ kg ⁻¹)	1.83x10 ⁵⁸	4.47x10 ⁵⁸	5.17x10 ⁵⁸	2.62x10 ⁵⁸	3.43x10 ⁵⁸
ω_p (Hz)	7.27x10 ¹⁵	1.13x10 ¹⁶	1.22x10 ¹⁶	8.72x10 ¹⁵	9.96x10 ¹⁵
s_0 (x10 ¹³ m ⁻²)	2.00x10 ¹³	2.17x10 ¹³	1.92x10 ¹³	2.00x10 ¹³	2.71x10 ¹³
λ_0 (x10 ⁻⁷ m)	1.93x10 ⁻⁰⁷	1.93x10 ⁻⁰⁷	1.94x10 ⁻⁰⁷	1.93x10 ⁻⁰⁷	1.90x10 ⁻⁰⁷

The first and third order of the transition moment (M_{-1} and M_{-3}) of the optical spectrum of ZnO/PVDF-TrFE nanocomposite samples are calculated and listed in Table 5 as follows [53]:

$$E_0^2 = \frac{M_{-1}}{M_{-3}} \quad \text{and} \quad E_d^2 = \frac{M_{-1}^3}{M_{-3}} \quad (20)$$

The embedding of ZnO NPs into the matrix of PVDF-TrFE with various concentrations increases the molecular size and consequently the polarizability volume (μ') will increase.

The values of average oscillator strength (s_0) and average interband oscillator wavelength (λ_0) of ZnO/PVDF-TrFE nanocomposites can be determined by the following equations [56],

$$\frac{n_0^2 - 1}{n^2 - 1} = 1 - \left(\frac{\lambda_0}{\lambda} \right)^2 \quad (22)$$

$$n^2 - 1 = \frac{s_0 \lambda_0^2}{\left(1 - \frac{\lambda_0^2}{\lambda^2} \right)} \quad (23)$$

where $s_0 = (n_0^2 - 1) / \lambda_0^2$. Fig.10b illustrates the variation of $(n^2 - 1)^{-1}$ versus λ^{-2} . Values of λ_0 and s_0 are estimated from the intercept ($1/s_0 \lambda_0^2$) and slope ($-1/s_0$) of the curves of Fig. 10b and given in Table 5. It is found that, λ_0 and s_0 values are of the typical order as those found for various materials based on SOM [44, 56].

3.5.3 Dielectric properties

The concentration of carriers to its effective mass (N/m^*) ratio and the lattice dielectric constant (ϵ_L) are estimated by using an equation contains the refractive index (n) depend on the wavelength (λ) as follows [57]:

$$n^2 = \epsilon_L - \frac{e^2}{4\pi \epsilon_0 c^2} \left(\frac{N}{m^*} \right) \lambda^2 \quad (24)$$

Fig. 10c depicts the dependence of n^2 on λ^2 . Values of ϵ_L and N/m^* are calculated from the slope and intercept of the fitted lines, as presented in Fig. 10c. It is found that the ZnO/PVDF-TrFE nanocomposites have higher values of ϵ_L than of pure PVDF-TrFE. Since the parameters ϵ_L and N/m^* contribute to the polarization process of materials, the observed variation in the values of these parameters with increasing the content of ZnO NPs support promising results for the nonlinear optical (NLO) properties [58]. Furthermore, ϵ_L values are found to be higher than the values of ϵ_s , and this difference may be due to the change in the carrier concentrations [11, 51, 59]. Moreover, the values of plasma frequency (ω_p) are computed for all samples and given in Table 5 using the following formula:

$$\omega_p = \sqrt{\frac{e^2}{\epsilon_0} \left(\frac{N}{m^*} \right)} \quad (25)$$

The higher values of (ω_p) as given in Table 5 is attributed to the higher values of (N/m^*) due to the increase in ZnO NPs content.

The optical dielectric constant is correlated with the density of states (DOS) in the band gap, and consequently it gives valuable information regarding the structure of bands in the material.

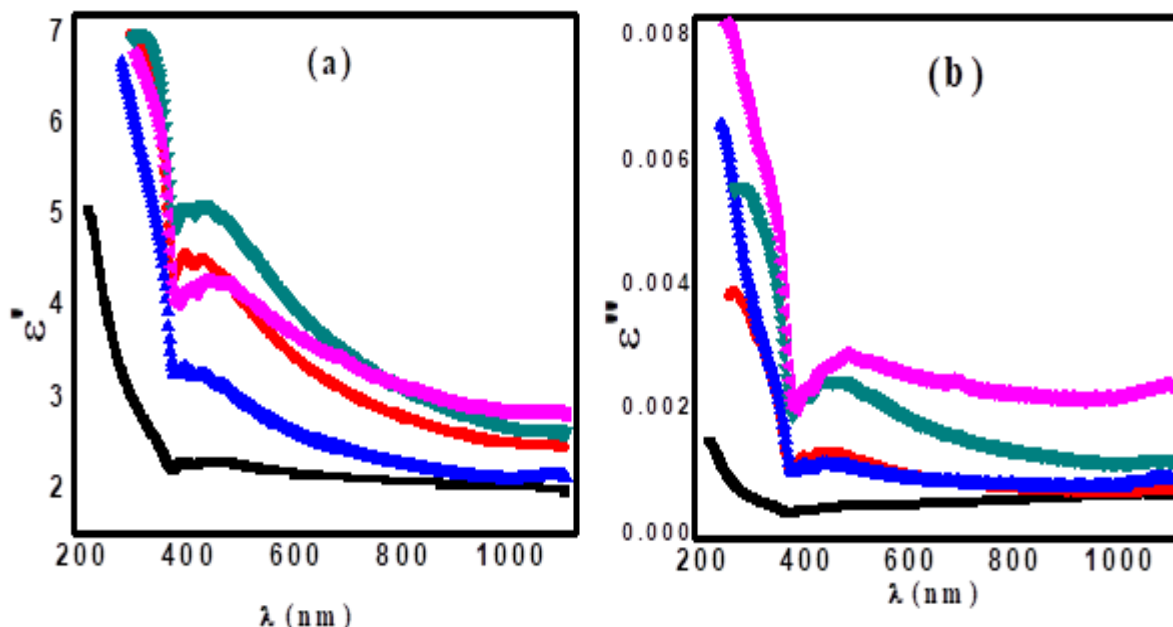


Fig. 11: a) ϵ' versus λ and b) ϵ'' versus λ . (■) PVDF-TrFE, (●) 0.5 wt% ZnO/PVDF-TrFE, (▲) 0.75 wt% ZnO/PVDF-TrFE, (▼) 1 wt% ZnO/PVDF-TrFE and (◄) 1.25 wt% ZnO/PVDF-TrFE.

The complex dielectric constant $\varepsilon^*(\omega)$ is expressed as follows:

$$\varepsilon^*(\omega) = \varepsilon' + i\varepsilon'' \quad (26)$$

where ε' is the dielectric constant and ε'' is the dielectric loss, respectively and can be estimated using the following equations[51, 60]:

$$\begin{aligned} \varepsilon' &= n^2 - k^2 \\ \varepsilon'' &= 2nk \end{aligned} \quad (27)$$

Fig. 11 shows the dependence of ε' and ε'' on the wavelength. It is found ε' and ε'' changed with the same trend versus the wavelength, with much higher values of ε' than ε'' values. Generally, values of ε' of ZnO/PVDF-TrFE nanocomposites are found to be larger than that of pure PVDF-TrFE. This confirms the existence of more density of states (DOS) which, in turn, enhances the polarization and consequently the dielectric constant of the nanocomposite samples will increase. It is observed at $\lambda=300$ nm ($h\nu = 4.13$ eV) the values of ε' and ε'' are changed from 2.9 and 5.29×10^{-4} of pure PVDF-TrFE to 6.97 and 6.49×10^{-4} for ZnO/PVDF-TrFE nanocomposite, as shown in Fig. 11a. The attitude of ε' exhibited a dispersion region below $\lambda = 400$ nm (3.1 eV). This dispersion may be ascribed to the polar nature of PVDF-TrFE after enhancing the electroactive β -phase fraction with increasing the content of ZnO. This region of dispersion has a major role in the optical communications and optical devices design [61]. Furthermore, the molecules at higher wavelengths cannot follow the incident field fluctuations and hence ε' tends to be constant [62].

Fig. 11b illustrates the variation of dielectric loss (ε'') against wavelength.

It is evident that values of ε'' of ZnO/PVDF-TrFE nanocomposites are larger than those of pure PVDF-TrFE. In fact, the dielectric loss describes the energy absorbed within the material owing to the dipolar motion and its higher values at lower wavelength (higher photon energy) may be related to the formation of the dipoles that are produced after incorporating ZnO NPs in the matrix of PVDF-TrFE.

3.5.4 Nonlinear optical (NLO) properties

The study of nonlinear optical (NLO) parameters of ZnO/PVDF-TrFE nanocomposites is important for different applications such as optoelectronic circuits, optical switching devices optical modulators and processors [58, 63]. When the material is exposed to an intense light beam, the phenomenon of nonlinearity will arise because of the net polarization that has been developed in the material. The dipole moment (P) and the susceptibility (χ) are correlated to each other, i.e., $P = \varepsilon_0 \chi E$, where E is the strength of the electric field. The susceptibility contains nonlinear and linear susceptibilities, i.e., $\chi = \chi^L + \chi^{NL}$, where $\chi^L = \chi^1$ represents the linear portion of the susceptibility and $\chi^{NL} = \chi^2 + \chi^3$ represents the nonlinear portions of the susceptibility.

$$P = \chi^1 E + \chi^2 E + \chi^3 E \quad (28)$$

where the significant terms are linear (χ^1) and nonlinear cubic order (χ^3) susceptibilities and can be expressed in terms of the linear refractive index (n_0) as follows;

Table 6. Linear and nonlinear optical parameters values of ZnO/PVDF-TrFE nanocomposites.

Optical Parameter	PVDF-TrFE	0.5 wt% ZnO/PVDF-TrFE	0.75 wt% ZnO/PVDF-TrFE	1.0 wt% ZnO/PVDF-TrFE	1.25 wt% ZnO/PVDF-TrFE
χ^1	0.076	0.099	0.223	0.116	0.127
χ^3 (esu)	6.24×10^{-15}	1.76×10^{-14}	4.43×10^{-13}	3.23×10^{-14}	4.65×10^{-14}
n_2	1.67×10^{-13}	4.41×10^{-13}	8.56×10^{-12}	7.76×10^{-13}	1.09×10^{-12}

$$\chi^1 = (n_0^2 - 1) / 4\pi$$

$$\chi^3 = A(\chi^1)^4 = \frac{A}{(4\pi)^4} (n_0^2 - 1)^4$$

and

(29)

where A is a constant = 1.79×10^{-10} esu. Also, the nonlinear refractive index (n_2) is estimated using χ^3 as follows [64]:

$$n_2 = \frac{12\pi\chi^3}{n_0} \quad (30)$$

χ^1 , χ^3 and n_2 values are determined and given in Table 6.

It is noted that all the linear and nonlinear optical parameters are enhanced and increased with increasing the concentration of ZnO NPs indicating a structure modification in the matrix of PVDF-TrFE has been occurred.

3.5.5 Optical and electrical conductivity

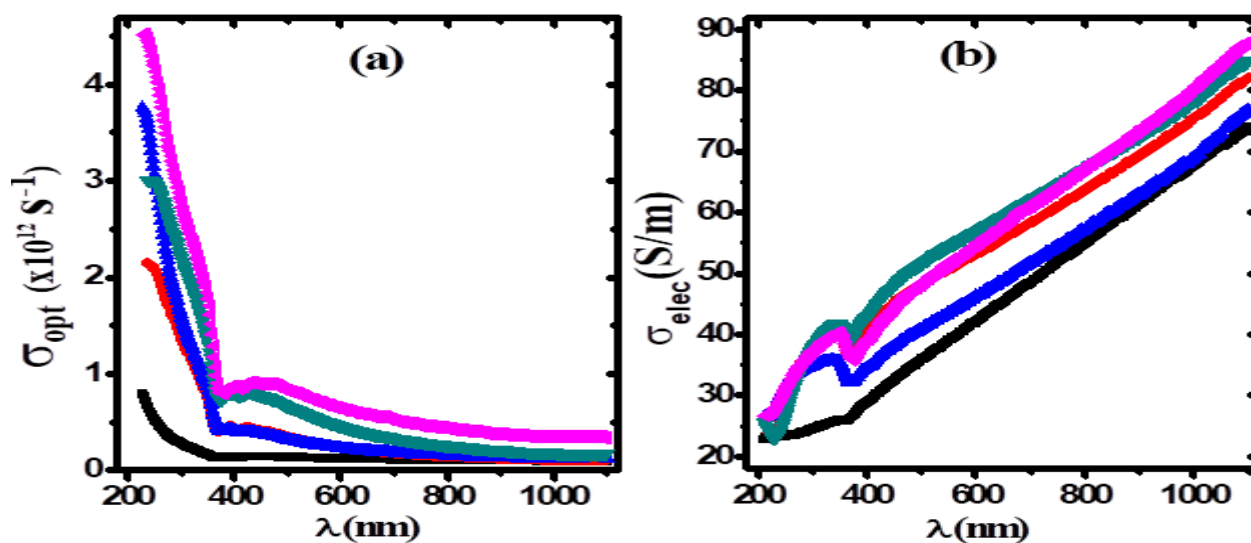


Fig. :12 a) σ_{opt} versus λ and b) σ_{elec} versus λ . (■) PVDF-TrFE, (●) 0.5 wt% ZnO/PVDF-TrFE, (▲) 0.75 wt% ZnO/PVDF-TrFE, (▼) 1 wt% ZnO/PVDF-TrFE and (◀) 1.25 wt% ZnO/PVDF-TrFE.

The optical and electrical conductivity (σ_{opt} and σ_{elec}) of ZnO/PVDF-TrFE nanocomposites are estimated by the following formula [65]:

$$\sigma_{opt} = \frac{\alpha n c}{4\pi}$$

$$\sigma_{elec} = \frac{2\lambda\sigma_{opt}}{\alpha} \quad (31)$$

Fig. 12 shows the dependence of optical and electrical conductivity on wavelength for all samples. It is observed that the samples have a maximum optical conductivity value in UV region (high absorption region), followed by a decrease in conductivity with increasing wavelength, and the conductivity tends to saturate at high wavelengths, as shown in Fig. 12a. High values of the optical conductivity are ascribed to the excited electrons by the photon energy, while the decrease in σ_{opt} is due to the reduction of the excited electrons. Furthermore, values of σ_{opt} are found to be ZnO NPs content dependent, i.e., it increased with increasing ZnO NPs. This variation in the optical conductivity can be interpreted in terms of the defects present in the nanocomposite samples. After adding ZnO NPs into the matrix of PVDF-TrFE some defects will form therefore, such defects will produce localized states in the band gap of the samples.

The band gap will reduce due to the higher concentration of localized states and thus increase the optical conductivity. On the other hand, the electrical conductivity displayed an opposite trend to the optical conductivity, as shown in Fig. 12b. It is found that the σ_{elec} is increased with increasing the

wavelength and as well as the content of ZnO NPs and changed from 23 S/cm for PVDF-TrFE to 89 S/cm for 1.25 wt% ZnO/PVDF-TrFE NCs composite sample, revealing the semiconducting nature of the ZnO/PVDF-TrFE nanocomposites.

3.6 Piezoelectric activity

The PVDF and its copolymers crystal structure showing strong impact in the study of the piezoelectric behavior. It is known that owing to the parallel arrangement of the molecular chains, the unit cell of α -phase does not have a net dipole moment. On the other hand, the unit cell in β -phase has a net dipole moment, because the dipoles in this phase are perpendicular to the molecular chain axis and parallel to each other hence it can be spontaneously polarized. Since the β phase is the most ideal phase structure, the β phase content has the most obvious influence on the piezoelectric activity of PVDF-TrFE copolymer [66]. The electric polarization value (P) is proportional to the applied stress σ as follows

$$P = d \sigma \quad (32)$$

Where d is the piezoelectric parameter coefficient and due to the unit cell symmetry can be expressed as follows [67]:

$$d_{ij} = \begin{bmatrix} 0 & 0 & 0 & d_{15} & 0 \\ 0 & 0 & d_{24} & 0 & 0 \\ d_{31} & d_{32} & d_{33} & 0 & 0 \end{bmatrix} \quad (33)$$

Where, the subscript “ i ” refers to the electric field direction, while, “ j ” refers to the stress or strain direction. The piezoelectric coefficient (d_{33}) can be estimated as follows:

$$d_{33} = \frac{1}{A} \left(\frac{\partial Q}{\partial \sigma} \right) \quad (34)$$

Where A and Q are the area of the sample and released charge, respectively. Fig. 13(a&b) displays the piezoelectric coefficient (d_{33}) dependence on the applied stress at various measuring temperatures for PVDF-TrFE and 1.25 wt% ZnO/PVDF-TrFE nanocomposite sample.

In general, the data of piezoelectric coefficient of PVDF-TrFE and ZnO/PVDF-TrFE nanocomposites are dependence on stress and temperature dependent. The piezoelectric coefficient is found to increase nonlinearly with the applied stress increasing. It is found that the piezoelectric coefficient d_{33} of PVDF-TrFE is enhanced from 9.94 PC/N to 19.03 PC/N for ZnO/PVDF-TrFE nanocomposite sample at $\sigma=6.24 \times 10^5$ Pa. Similar behavior of stress-dependent piezoelectric coefficient has been reported previously [68]. Based on the dimensional effect model, the inter-chain distance could be changed more easily than the length of the covalently bonded chain by an external stress. As a consequence, d_{33} is likely to have a stronger dependence on the applied stress [69].

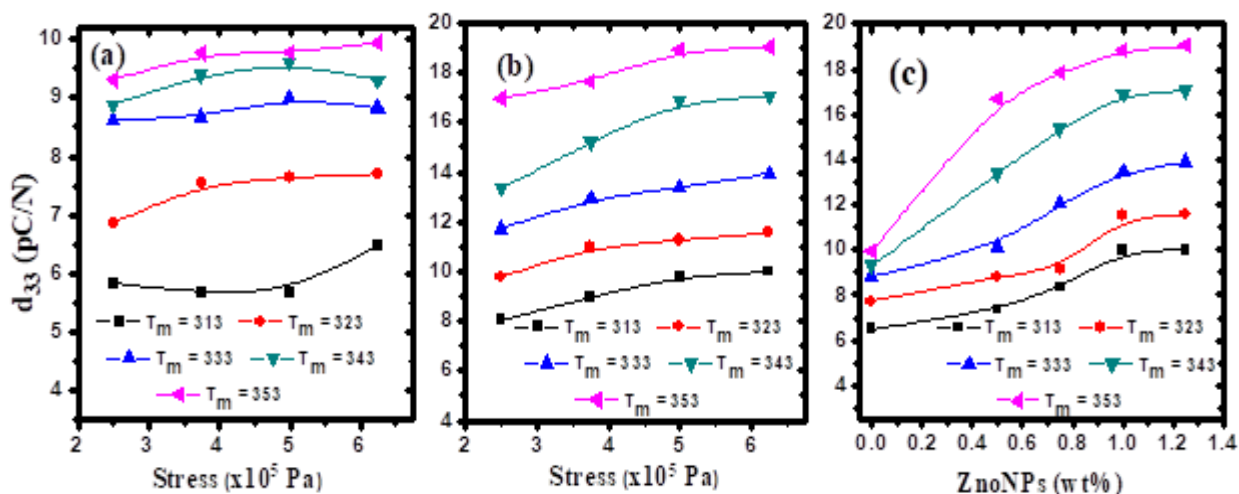


Fig. 13: The piezoelectric coefficient (d_{33}) against the stress at different measuring temperatures for a) pure PVDF-TrFE b) 1.25 wt% ZnO/PVDF-TrFE and c) d_{33} versus ZnO NPs ratio. The samples are poled with $E_p=1 \times 10^7$ V/m at $T_p=353$ K for $t_p=20$ min and the applied stress is 6.24×10^5 Pa.

When a stress is applied to the sample, an instantaneous in-plane strain is induced and the center of positive ions and negative ions charges will be changed. Hence, more dipoles will be rotated upward, causing an increase in polarization, ΔP , resulting in an effective electric field in the sample plane. This electromechanical interaction is actually the cause of the high piezoelectricity of the samples [70].

Also, the d_{33} values increase with increasing measurement temperatures (T_m) for all samples. For higher temperature the mobility of the molecular chain will increase, making the dipoles moments align better with the applied electric field, thus increasing the piezoelectric [71].

Fig. 13c depicts the piezoelectric coefficient d_{33} dependence on the content of ZnO NPs at various maximum temperatures and stress value of 6.24×10^5 Pa. It is observed that the values of d_{33} enhanced nonlinearly and tends to saturate at higher concentration of ZnO NPs.

This may be because the saturation of the ferroelectric domains in the ZnO/PVDF-TrFE nanocomposites. PVDF is a semi-crystalline polymer and is synthesized by the polymerization process of $CF_2=CH_2$ monomers. Defects will occur in the polymer main chain when two CF_2 or CH_2 groups are connected.

The addition of fillers such as nanoparticles (NPs), graphene oxide (GO), dyes and CNTs for obtaining PVDF copolymer composites is an important practical method for show good improvement of the piezoelectric properties of PVDF[72]. Therefore, the increased defects in the polymeric chain of the ZnO/PVDF-TrFE nanocomposite samples after embedding ZnO NPs will increase the polarization of the semi-crystalline polymer film, which in turn will increase the piezoelectric response.

It can be said that increasing the ZnO content increased the β -phase content in the nanocomposite samples and thus enhanced the piezoelectric response [73]. The defects in the polymer matrix due to introduce ZnO nanoparticles

that produce good polarity and polarization in the semi crystalline copolymer and enhance the piezoelectric response [74- 75].

4. Conclusion

Nonocomposites of PVDF-TrFE and ZnO are prepared by the casting method. The interaction between PVDF-TrFE and ZnO is investigated by various techniques. Data analysis of XRD pattern showed that the electroactive β -phase fraction is enhanced and the structural parameters such as crystal size, lattice internal strain and dislocation density are affected by the increasing the content of ZnO NPs. Analysis of FTIR data showed that the electroactive β -phase fraction is enhanced according to the interactivity between the ZnONPs and PVDF-TrFE matrix. DSC measurements showed that the temperature of ferroelectric-paraelectric phase transition is decreased from 404 K to 377 K and the melting temperature from 423 to 417 K for PVDF-TrFE to 1.25 wt% ZnO/PVDF-TrFE nanocomposite, respectively. TGA analysis revealed that the thermal stability of PVDF-TrFE has been enhanced with increasing the content of ZnO NPs and the enthalpy-entropy compensation (EEC) influence has been verified. Measurements of UV showed that with increasing ZnONPs content the E_U values increase while both E_{ig} and E_{dg} values decrease from 2.89 eV and 4.82 eV for pure PVDF-TrFE to 1.69 eV and 3.85 eV for 1.25 wt% ZnO/PVDF-TrFE, respectively. The variations of E_U , E_{ig} and E_{dg} values are attributed to the structure modification. Parameters of nonlinear and linear optical of PVDF-TrFE are computed and interpreted according to the single-oscillator model. It is noted that the values of these parameters are enhanced with increasing ZnONPs content. These advantages make ZnO/PVDF-TrFE nanocomposites are strong candidates for potential applications such as nonlinear optics (NLO). The piezoelectric activity data revealed that the coefficient d_{33} of PVDF-TrFE is enhanced and increased from 9.94 PC/N to 19.03 PC/N for ZnO/PVDF-TrFE nanocomposites. The enhancement and improvement of the d_{33} values with ZnO NPs content increase can be attributed to the high polarization. Thus, ZnO/PVDF-TrFE nanocomposites can be candidate for high energy storage systems.

Conflict of interest

They should state there is no conflict of interest. It should be stated clearly before Acknowledgements

Acknowledgment

This work was performed under the financial support of our project from “Research Unit of Mansoura University, MU-SCI-21-23”

References

1. Hafner, J.; et al. Origin of the strong temperature effect on the piezoelectric response of the ferroelectric (co-) polymer P (VDF70-TrFE30). *Polymer*.**2019**, 170, 1-6. <https://doi.org/10.1016/j.polymer.2019.02.064>
2. Sung, M.; et al. A micro-machined hydrophone employing a piezoelectric body combined on the gate of a field-effect transistor. *Sensors and Actuators A: Physical*.**2016**, 237, 155-166. <https://doi.org/10.1016/j.sna.2015.11.025>
3. Jun Li, D.; et al. Polymer piezoelectric energy harvesters for low wind speed. *Applied Physics Letters*.**2014**, 104(1), 012902. <https://doi.org/10.1063/1.4861187>
4. Xie, L.; et al. Properties and applications of flexible poly (vinylidene fluoride)-based piezoelectric materials. *Crystals*.**2021**, 11(6), 644. <https://doi.org/10.3390/cryst11060644>
5. Soulestin, T.; et al. Vinylidene fluoride-and trifluoroethylene-containing fluorinated electroactive copolymers. How does chemistry impact properties?. *Progress in Polymer Science*.**2017**, 72, 16-60. <https://doi.org/10.1016/j.progpolymsci.2017.04.004>
6. Hassan, A.; Habib, A.; Abdelhamid, M. I.; Fahmy, T.; Sarhan, A. Investigation of Piezoelectric Effect and Thermally Stimulated Depolarization Current of Poly (Vinyl Chloride-co-Vinyl Acetate-co-2-Hydroxypropyl Acrylate)/Poly (Vinylidene Fluoride-Trifluoroethylene) Polymer Blend. *Ferroelectrics*.**2023**, 613. DOI: 10.1080/00150193.2023.2215514
7. Oliveira, F.; et al. Process influences on the structure, piezoelectric, and gas-barrier properties of PVDF-TrFE copolymer. *J. Polym. Sci. Part B: Polym. Phys.*, **2014**, 52(7), 496-506. <https://doi.org/10.1002/polb.23443>
8. El-Hami, K.; et al. Structural analysis of the P (VDF/TrFE) copolymer film. *Chemical engineering science*.**2003**, 58(2), 397-400. [https://doi.org/10.1016/S0009-2509\(02\)00521-3](https://doi.org/10.1016/S0009-2509(02)00521-3)
9. Rozenberg, B.; Tenne, R. Polymer-assisted fabrication of nanoparticles and nanocomposites. *Progress in polymer science*.**2008**, 33(1), 40-112. <https://doi.org/10.1016/j.progpolymsci.2007.07.004>
10. Sarhan, A.; Fahmy, T. Optical properties, antibacterial activity, and relaxation behavior investigation of chitosan/green synthesized silver nanoparticles by thermally stimulated depolarization current technique. *Polymer Science, Series B*.**2021**, 63, 578-590. <https://doi.org/10.1134/S1560090421050110>
11. Fahmy, T.; Sarhan, A. Investigation of optical properties and antibacterial activity of chitosan copper nanoparticle

- composites. *Materials Technology*. **2022**, 37(12), 2400-2413. <https://doi.org/10.1080/10667857.2022.2038497>
12. Indolia, A. P.; Gaur, M. J. Optical properties of solution grown PVDF-ZnO nanocomposite thin films. *Journal of Polymer Research*. **2013**, 20, 1-8. <https://doi.org/10.1007/s10965-012-0043-y>
 13. Shepelin, N. A.; et al. New developments in composites, copolymer technologies and processing techniques for flexible fluoropolymer piezoelectric generators for efficient energy harvesting. *Energy & Environmental Science*. **2019**, 12(4), 1143-1176. DOI: [10.1039/C8EE03006E](https://doi.org/10.1039/C8EE03006E)
 14. Dimitry, O. I.; et al. Preparation and properties of elastomeric polyurethane/organically modified montmorillonite nanocomposites. *Journal of polymer research*. **2010**, 17, 801-813. <https://doi.org/10.1007/s10965-009-9371-y>
 15. Kumar, M.; et al. P(VDF-TrFE)/ZnO nanofiber composite based piezoelectric nanogenerator as self-powered sensor: fabrication and characterization. *Journal of Polymer Research*. **2022**, 29, 44. <https://doi.org/10.1007/s10965-022-02890-1>
 16. Liang, S.; et al. A novel ZnO nanoparticle blended polyvinylidene fluoride membrane for anti-irreversible fouling. *J. membrane Sci.*, **2012**, 394, 184-192. <https://doi.org/10.1016/j.memsci.2011.12.040>
 17. Sui, X.; Shao, C.; Liu, Y. White-light emission of polyvinyl alcohol/ ZnO hybrid nanofibers prepared by electrospinning. *Applied Physics Letters*. **2005**, 87(11), 1131-1135. <https://doi.org/10.1063/1.2048808>
 18. Kumar, A.P.; et al. Nanoscale particles for polymer degradation and stabilization—trends and future perspectives. *Progress in polymer science*. **2009**, 34(6), 479-515. <https://doi.org/10.1016/j.progpolymsci.2009.01.002>
 19. Ahmed, M.; et al. Preparation and characterization of ZnO nanoparticles by simple precipitation method. *Inter. J. of Science, Engineering and Technology*. **2016**, 4(3), 507-512.
 20. Polat, K. Energy harvesting from a thin polymeric film based on PVDF-HFP and PMMA blend. *Appl. Phys. A*. **2020**, 126, 1-8. <https://doi.org/10.1007/s00339-020-03698-w>
 21. Lei, T.; et al. Spectroscopic evidence for a high fraction of ferroelectric phase induced in electrospun polyvinylidene fluoride fibers. *RSC Advances*. **2013**, 3(47), 24952-24958. DOI: [10.1039/C3RA42622J](https://doi.org/10.1039/C3RA42622J)
 22. Kumar, M.; kumari, P.; sahatiya, P. PVDF-TrFE/ZnO nanofiber composite based piezoelectric nanogenerator as self-powered sensor: fabrication and characterization. *Journal of Polymer Research*. **2022**, 29, 44. <https://doi.org/10.1007/s10965-022-02890-1>
 23. Pratihari, S.; et al. Enhanced dielectric, ferroelectric, energy storage and mechanical energy harvesting performance of ZnO–PVDF composites induced by MWCNTs as an additive third phase. *Soft Matter*. **2021**, 17(37), 8483-8495. DOI: [10.1039/D1SM00854D](https://doi.org/10.1039/D1SM00854D)

24. Luo, Y.; et al. Effect of aluminium nitrate hydrate on the crystalline, thermal and mechanical properties of poly (vinyl alcohol) film. *Polymers and Polymer Composites*. **2015**, 23(8), 555-562. DOI: [10.1177/096739111502300805](https://doi.org/10.1177/096739111502300805)
25. Kundu, P.P.; et al. Influence of film preparation procedures on the crystallinity, morphology and mechanical properties of LLDPE films. *European Polymer Journal*. **2003**, 39(8), 1585-1593. DOI: [10.1016/S0014-3057\(03\)00056-9](https://doi.org/10.1016/S0014-3057(03)00056-9)
26. Das, S.; et al. Tuning the nonlinear susceptibility and linear parameters upon annealing Ag_{60-x}Se₄₀Te_x nanostructured films for nonlinear and photonic applications. *Materials Advances*. **2022**, 3(20), 7640-7654. DOI: [10.1039/D2MA00646D](https://doi.org/10.1039/D2MA00646D)
27. Suresh, R., V.; et al. Applied Surface Science Effect of annealing temperature on the microstructural, optical and electrical properties of CeO₂ nanoparticles by chemical precipitation method. *Applied Surface Science*. **2013**, 273, 457-464. DOI: [10.1016/j.apsusc.2013.02.062](https://doi.org/10.1016/j.apsusc.2013.02.062)
28. Mandal, D.; et al. Bandgap determination of P (VDF-TrFE) copolymer film by electron energy loss spectroscopy. *Bulletin of Mater. Sci.*, **2010**, 33, 457-461. DOI: [10.1007/s12034-010-0070-4](https://doi.org/10.1007/s12034-010-0070-4)
29. Janakiraman, S.; et al. Electroactive poly (vinylidene fluoride) fluoride separator for sodium ion battery with high coulombic efficiency. *Solid State Ionics*. **2016**, 292, 130-135. <https://doi.org/10.1016/j.ssi.2016.05.020>
30. Imai, Y.; Kimura, Y.; Niwano, M. Organic hydrogen gas sensor with palladium-coated β -phase poly (vinylidene fluoride) thin films. *Applied Physics Letters*. **2012**, 101(18), 181907. <https://doi.org/10.1063/1.4764064>
31. Li, L.; et al. Studies on the transformation process of PVDF from α to β phase by stretching. *Rsc Advances*. **2014**, 4(8), 3938-3943. DOI: [10.1039/C3RA45134H](https://doi.org/10.1039/C3RA45134H)
32. Kasbi, S. F.; et al. β -Polymorph enhancement in poly (vinylidene fluoride) by blending with polyamide 6 and barium titanate nanoparticles. *Journal of Applied Polymer Science*. **2020**, 137(45), 49403. <https://doi.org/10.1002/app.49403>
33. Ahmad, A.; Farooqui; U.; Hamid, N. Porous (PVDF-HFP/PANI/GO) ternary hybrid polymer electrolyte membranes for lithium-ion batteries. *RSC advances*. **2018**, 8(45), 25725-25733. DOI: [10.1039/C8RA03918F](https://doi.org/10.1039/C8RA03918F)
34. Madorskaya, L. Y.; et al. Role of end groups in polyvinylidene fluoride. *Polymer Science USSR*. **1983**, 25(10), 2490-2496. [https://doi.org/10.1016/0032-3950\(83\)90186-7](https://doi.org/10.1016/0032-3950(83)90186-7)
35. Dias, J.; et al. Thermal degradation behavior of ionic liquid/fluorinated polymer composites: Effect of polymer type and ionic liquid anion and cation. *Polymer*. **2021**, 229, 123995. <https://doi.org/10.1016/j.polymer.2021.123995>
36. Zulfiqar, S.; et al. Study of the thermal degradation of polychlorotrifluoroethylene, poly (vinylidene fluoride) and copolymers of chlorotrifluoroethylene and vinylidene

- fluoride. *Polym. Deg. Stab.*, **1994**, 43(3), 423-430.
[https://doi.org/10.1016/0141-3910\(94\)90015-9](https://doi.org/10.1016/0141-3910(94)90015-9)
37. Li, C.; et al. Non-isothermal crystallization behaviors and spherulitic morphology of poly (lactic acid) nucleated by a novel nucleating agent. *Journal of Thermal Analysis and Calorimetry*. **2015**, 122, 407-417.
 DOI 10.1007/s10973-015-4677-y
38. Chrissafis, K. Kinetics of thermal degradation of polymers: complementary use of isoconversional and model-fitting methods. *Journal of Thermal Analysis and Calorimetry*. **2009**, 95, 273-283.
 DOI:10.1007/s10973-008-9041-z
39. Vlaev, L.; Markovska, I.; Lyubchev, L. Non-isothermal kinetics of pyrolysis of rice husk. *Thermochimica acta*. **2003**, 406(1-2), 1-7. [https://doi.org/10.1016/S0040-6031\(03\)00222-3](https://doi.org/10.1016/S0040-6031(03)00222-3)
40. Coats, A. W. Kinetic parameters from thermogravimetric data. *Nature*. **1964**, 201, 68.
<https://doi.org/10.1038/201068a0>
41. Hamid, S.; HUSSAIN, I. Handbook of polymer Degradation. Revised and expanded. Edited by Hamid, SH Marcel Dekker. Inc., New York. **2000**.
42. Liu, L.; Guo, Q. Isokinetic relationship, isoequilibrium relationship, and enthalpy-entropy compensation. *Chemical Reviews*. **2001**, 101(3), 673-696.
<https://doi.org/10.1021/cr990416z>
43. Ahmed, M.; Fahmy, T. Alpha relaxation study of poly (vinyl chloride co-vinylacetate-co-2-hydroxypropyl acrylate). *Polymer-Plastics Technology and Engineering*. **2005**, 44(8-9), 1559-1572.
 DOI: 10.1080/03602550500209507
44. Elmahdy, M.; et al. Thermal degradation and optical characteristics of plasticized poly (vinyl chloride-co-vinyl acetate-co-2-hydroxypropyl acrylate) terpolymer. *J. of Materials Science: Materials in Electronics*. **2022**, 33(30), 23639-23658.
<http://dx.doi.org/10.1007/s10854-022-09124-6>
45. Elsharkawy, W.; et al. Effect of γ -irradiation on thermally stimulated depolarization current spectra of polyethylene-grafted-poly (Acrylic acid). *Radiation Effects and Defects in Solids*. **2022**, 177(7-8), 671-687.
<https://doi.org/10.1080/10420150.2022.2073880>
46. Srivastava, A.; Virk, H. 50 MeV lithium ion beam irradiation effects in poly vinylidene fluoride (PVDF) polymer. *Bulletin of Mater. Sci.*, **2000**, 23, 533-538.
 DOI:10.1007/BF02903896
47. Rekik, H.; et al. Dielectric relaxation behaviour in semi-crystalline polyvinylidene fluoride (PVDF)/TiO₂ nanocomposites. *Composites Part B: Engineering*. **2013**, 45(1), 1199-1206.
<https://doi.org/10.1016/j.compositesb.2012.08.002>
48. Urbach, F. The long-wavelength edge of photographic sensitivity and of the electronic absorption of solids. *Physical Review*. **1953**, 92(5), 1324.
 DOI: <https://doi.org/10.1103/PhysRev.92.1324>
49. Lucovsky, G.; Nemanich, R.; Galeener, F. Amorphous and Liquid

- Semiconductors. Springer Science & Business Media. **1972**.
50. W. B. Elsharkawy, T.F., M. A. Azzam, A. Habib and Afaf Sarhan, Structural and Optical Properties of Poly (Vinyl Alcohol)/Copper Nanocomposites Prepared by an Eco-friendly Electrochemical Method. *Biointerface Research in Applied Chemistry*. **2023**, 13.
<https://doi.org/10.33263/BRIAC13X.000>
51. Ahmed, M.; et al. Linear and Non-linear Optical Parameters of Copper Chloride Doped Poly (Vinyl Alcohol) for Optoelectronic Applications. *Egyptian Journal of Chemistry*. **2022**, 65(9), 99-108. DOI: [10.21608/EJCHEM.2022.105927.4878](https://doi.org/10.21608/EJCHEM.2022.105927.4878)
52. Wemple, S. Refractive-index behavior of amorphous semiconductors and glasses. *Physical Review B*. **1973**, 7(8), 3767. <https://doi.org/10.1103/PhysRevB.7.3767>
53. Wemple, S.; DiDomenico Jr, M. Behavior of the electronic dielectric constant in covalent and ionic materials. *Physical Review B*. **1971**, 3(4), 1338. <https://doi.org/10.1103/PhysRevB.3.1338>
54. Atkins, P.; Atkins, P. W.; de Paula, J. Atkins' physical chemistry. *Oxford university press*. **2014**.
55. Izgorodina, E. I.; Forsyth, M.; MacFarlane, D. On the components of the dielectric constants of ionic liquids: ionic polarization?. *Physical chemistry chemical physics*. **2009**, 11(14), 2452-2458. DOI: [10.1039/B815835E](https://doi.org/10.1039/B815835E)
56. Yakuphanoglu, F.; Cukurovali, A.; Yilmaz, I. Single-oscillator model and determination of optical constants of some optical thin film materials. *Physica B: Condensed Matter*. **2004**, **353**(3-4), 210-216. <https://doi.org/10.1016/j.physb.2004.09.097>
57. Behera, M.; et al. Thermal annealing induced structural, optical and electrical properties change in As₄₀Se_{60-x}Bix chalcogenide thin films. *AIP Advances*. **2019**, 9(9), 095065. <https://doi.org/10.1063/1.5111019>
58. Sahoo, D.; et al. In situ laser irradiation: the kinetics of the changes in the nonlinear/linear optical parameters of As₅₀Se₄₀Sb₁₀ thin films for photonic applications. *RSC advances*. **2021**, 11(26), 16015-16025. DOI: [10.1039/D1RA02368C](https://doi.org/10.1039/D1RA02368C)
59. Fahmy, T.; Sarhan, A. Characterization and molecular dynamic studies of chitosan-iron complexes. *Bulletin of Mater. Sci.*, **2021**, 44(2), 142. <https://doi.org/10.1007/s12034-021-02434-1>
60. Yakuphanoglu, F.; et al. The refractive index dispersion and the optical constants of liquid crystal metal-free and nickel (II) phthalocyanines. *Physica B: Condensed Matter*. **2006**, 373(2), 262-266. <https://doi.org/10.1016/j.physb.2005.11.153>
61. Aslam, M.; Kalyar, M. A.; Raza, Z. A. Graphene oxides nanosheets mediation of poly (vinyl alcohol) films in tuning their structural and opto-mechanical attributes. *J. of Mater. Sci.: Mater. in Electronics*. **2017**, 28, 13401-13413. DOI [10.1007/s10854-017-7177-y](https://doi.org/10.1007/s10854-017-7177-y)
62. Elmahdy, M. M.; et al. Molecular dynamics and conduction mechanism of poly (vinyl chloride-co-vinyl acetate-co-2-hydroxypropyl acrylate) terpolymer containing ionic liquid. *Polymers*

- for *Advanced Technologies*. **2023**, 34(2), 800-816.
<https://doi.org/10.1002/pat.5932>
63. Elsharkawy, W. B.; Fahmy, T.; Azzam, M. A.; Habib, A.; Sarhan, A. Structural and Optical Properties of Poly (Vinyl Alcohol)/Copper Nanocomposites Prepared by an Eco-friendly Electrochemical Method. *Biointerface Res. Appl. Chem.* **2023**, 13. <https://doi.org/10.33263/BRIAC13X.000>
64. Knight, P. *Progress in Optics*. Vol. XXIII. *Taylor & Francis*. **1988**. <https://doi.org/10.1080/09500348814550061>
65. Banerjee, M.; Jain, A.; Mukherjee, G. Spectroscopic evaluation of optical parameters of a transition metal salt filled polymer material. *Defence Science Journal*. **2018**, 68(2), 225.
 DOI : 10.14429/dsj.68.12331
66. Sebastian, M.; et al. Understanding nucleation of the electroactive β -phase of poly (vinylidene fluoride) by nanostructures. *RSC advances*. **2016**, 6(114), 113007-113015.
 DOI: 10.1039/C6RA24356H
67. Wang, H.; et al. Piezoelectric, dielectric, and elastic properties of poly (vinylidene fluoride/trifluoroethylene). *J. of Appl. Phys.*, **1993**, 74(5), 3394-3398. <https://doi.org/10.1063/1.354566>
68. Habib, A.; et al. Enhancement of optical and piezoelectric properties of P (Vinylidene fluoride-hexafluoropropylene)/N, N-Dimethyl-4-nitro-4-Stilbenamine composites for optoelectronic applications. *Polymer-Plastics Technology and Materials*. **2022**, 61(18), 2001-2015. <https://doi.org/10.1080/25740881.2022.2086817>
69. Tashiro, K.; et al. Calculation of elastic and piezoelectric constants of polymer crystals by a point charge model: application to poly (vinylidene fluoride) form I. *Macromolecules*. **1980**, 13(3), 691-698. <https://doi.org/10.1021/ma60075a040>
70. Huang, Y.; et al. Enhanced piezoelectricity from highly polarizable oriented amorphous fractions in biaxially oriented poly (vinylidene fluoride) with pure β crystals. *Nature communications*. **2021**, 12(1), 675. <https://doi.org/10.1038/s41467-020-20662-7>
71. Cardoso, V.; et al. Improving the optical and electroactive response of poly (vinylidene fluoride-trifluoroethylene) spin-coated films for sensor and actuator applications. *Smart Materials and Structures*. **2012**, 21(8), 085020. DOI 10.1088/0964-1726/21/8/085020
72. Wu, L.; et al. Improved piezoelectricity of PVDF-HFP/carbon black composite films. *Journal of Physics D: Applied Physics*. **2014**, 47(13), 135302.
 DOI 10.1088/0022-3727/47/13/135302
73. Jones, G. D.; et al. Characterization, performance and optimization of PVDF as a piezoelectric film for advanced space mirror concepts. (No. SAND2005-6846). *Sandia National Laboratories (SNL), Albuquerque, NM, and Livermore, CA (United States)*. **2005**. <https://doi.org/10.2172/876343>
74. Elhadidy, H., et al., Structure and piezoelectricity of poly (styrene-co-acrylonitrile) copolymer doped with different dyes. *Polymer-Plastics*

Technology and Engineering. **2013**, 52(12),
1277-1284.

<https://doi.org/10.1080/03602559.2013.8146>

76

75. Abdelhamid, M., et al., Investigation of the structure and piezoelectricity of poly (vinylidene fluoride–trifluoroethylene) copolymer doped with different dyes. *International J. of Polym. Mater.* **2012**, 61(7), 505-519.

Doi: 10.1080/00914037.2011.593063